[Article] Signatures of Majorana bound states in transport properties of hybrid structures based on helical liquids

Signatures of Majorana bound states in transport properties of hybrid structures based on helical liquids

François Crépin,[1] Björn Trauzettel,[1] and Fabrizio Dolcini[2,3]
[1]*Institute for Theoretical Physics and Astrophysics, University of Würzburg, 97074 Würzburg, Germany*
[2]*Dipartimento di Scienza Applicata e Tecnologia, Politecnico di Torino, 10129 Torino, Italy*
[3]*CNR-SPIN, Monte Sant'Angelo, via Cintia, I-80126 Napoli, Italy*

(Received 20 January 2014; revised manuscript received 6 March 2014; published 15 May 2014)

Majorana bound states can emerge as zero-energy modes at the edge of a two-dimensional topological insulator in proximity to an ordinary s-wave superconductor. The presence of an additional ferromagnetic domain close to the superconductor can lead to their localization. We consider both normal-metal–superconductor (N-S) and Josephson (S-N-S) junctions based on helical liquids and study their spectral properties for arbitrary ferromagnetic scatterers in the normal region. Thereby, we explicitly compute Andreev wave functions at zero energy. We show under which conditions these states form localized Majorana bound states in N-S and S-N-S junctions. Interestingly, we can identify Majorana-specific signatures in the transport properties of N-S junctions and the Andreev bound levels of S-N-S junctions that are robust against external perturbations. We illustrate these findings with the example of a ferromagnetic double barrier (i.e., a quantum dot) close to the N-S boundaries.

DOI: 10.1103/PhysRevB.89.205115 PACS number(s): 74.45.+c, 74.78.Na, 71.10.Pm

I. INTRODUCTION

As main requirements for topological quantum computers, Majorana bound states (MBSs) in one-dimensional (1D) topological superconductors have been in the focus of recent research. Originally, MBSs where shown by Kitaev [1] to arise as localized edge states in a simple model of a 1D, spinless, p-wave superconductor [1], which is intimately related to the physics of spin-$\frac{1}{2}$ chains [2]. Subsequently, several groups proposed a possible experimental realization based on semiconductor nanowires with strong spin-orbit coupling, in proximity to an s-wave superconductor, and in the presence of a Zeeman field [3,4]. In order to probe MBS in transport experiments, hybrid structures, namely normal-metal–superconductor (N-S) and Josephson (S-N-S) junctions, have been realized with InAs nanowires that produced data compatible with Majorana physics [5–7]. Two kinds of transport signatures are generally considered. Tunnel current measurements in an N-S junction should lead to a robust zero-bias peak, signaling the presence of a zero-energy mode—the MBS—at the interface [8], while a fractional Josephson effect—a 4π periodic supercurrent mediated by localized MBS—is expected in S-N-S junctions [1]. Both results were reported in recent experiments [5–7], although the situation remains, to date, controversial [9–14]. Inspired by these experiments, remarkable attention has been devoted by theorists to the nanowire realizations. An interesting question is the fate of the localized MBS once contact is made with a normal lead, in either the N-S or the S-N-S case. Both numerical [15] and analytical [16] works showed that the Majorana states completely delocalize in the normal lead [15,16] and, in Josephson junctions, typically transform into Andreev states [15] for superconductor phase differences away from π. Such a delocalization is robust to the inclusion of Coulomb interactions [17].

Recent experiments [18,19] carried out on quantum spin Hall (QSH) insulators in proximity to s-wave superconductors may turn the tide. Without need for fine tuning, normal edge states of QSH insulators form a true helical liquid [20–24]. Furthermore, Dirac mass defects—such as the boundary between a ferromagnetic and a superconducting domain—can also host Majorana states [25,26]. In order to formulate precise predictions for transport experiments in N-S and S-N-S junctions based on helical liquids at the edge of topological insulators, it is crucial to have a deeper understanding of the formation of bound states. Specific situations have been investigated by some groups, such as Josephson junctions in the tunneling regime [26–29] or in the presence of isolated ferromagnetic impurities [30,31], magneto-Josephson effects [32], and N-S junctions with a quantum dot and a small Zeeman field [33]. However, a more general approach to the problem was missing so far. With this perspective in mind, we have derived a general result for the N-S and the S-N-S junctions with helical liquids in the presence of an *arbitrary* ferromagnetic domain, including, in particular, the case of two ferromagnetic barriers. More specifically, for the N-S case we have obtained a general formula for the Andreev reflection probability, which shows that, in addition to the zero excitation energy modes that are always perfectly Andreev reflected, many resonant, Fabry-Pérot-like peaks can appear at nonzero energies, related to virtual bound states at the ferromagnet-superconductor interface. As for the S-N-S case, we have determined the expression for the Andreev-bound levels, which shows that a zero-energy Andreev bound state at phase difference equal to π is stable, independent of the shape and strength of the ferromagnetic domain. Explicit results are shown for a ferromagnetic quantum dot realized by two sharp ferromagnetic barriers. Furthermore, for the particular case of a single ferromagnetic barrier of finite length, we provide explicit expressions of the Majorana wave functions, localized on either side of the barrier, in both N-S and S-N-S configurations.

Outline and summary of results. The paper is organized as follows. In Sec. II, we start by reviewing the spectral properties of the Bogoliubov-de Gennes theory for inhomogeneous superconductors in the case of broken spin rotation invariance. We discuss, in particular, the construction of Majorana states.

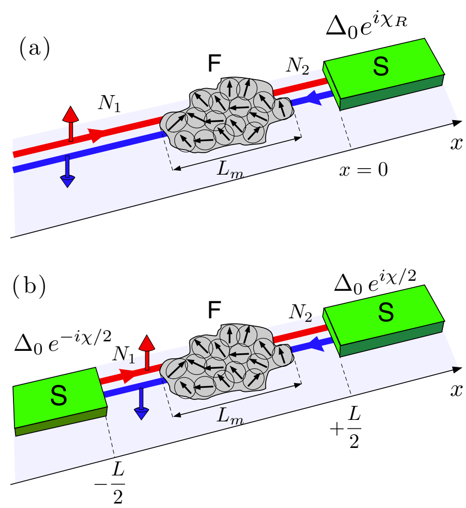

FIG. 1. (Color online) N-S and S-N-S junctions realized with helical edge states in the presence of a ferromagnetic domain F in the normal region. The regions N_1 and N_2 represent the interface regions where helical states propagate freely. Δ_0 is the pairing amplitude in the superconductor, χ_R the superconducting phase in the N-S setup, and χ the phase difference across the S-N-S junction.

In Sec. III, we investigate the transport properties of N-S junctions in the presence of a ferromagnetic scatterer and, in Sec. IV, we discuss properties of the Andreev bound levels for S-N-S junctions. In Sec. V, we discuss the implications of our findings for the detection of MBSs in experiments.

II. SPECTRAL PROPERTIES OF THE BOGOLIUBOV-DE GENNES THEORY

In this section, we review some general properties of the hybrid structures we shall consider thereafter. We derive the Bogoliubov-de Gennes Hamiltonian and proceed to discuss Andreev and Majorana states, introducing the notations we use in the later sections.

A. Hamiltonian of the system

We start by reviewing some general properties of the hybrid structures we shall consider thereafter. A helical liquid consists of a pair of edge states in a quantum spin Hall insulator (QSHI), where the group velocity is locked to the spin orientation. The helical liquid is contacted to one or two s-wave superconducting electrodes. Additionally, the presence of a ferromagnet along the edge induces an arbitrary Zeeman coupling in the normal region (see Fig. 1). The Hamiltonian of such a structure is given by

$$H = H_0 + H_Z + H_\Delta, \tag{1}$$

where H_0 is the Hamiltonian of the helical liquid, H_Z describes the Zeeman coupling, and H_Δ is the proximity-induced pairing potential. For definiteness, and without loss of generality, we assume that for the edge states the spin quantization axis is well defined and points along the z direction and that right- (left-) moving electrons are characterized by spin $\uparrow$ (spin $\downarrow$) so that

$$H_0 = \int dx\, (\psi^\dagger_{R\uparrow},\psi^\dagger_{L\downarrow})\,[v_F\, p_x\sigma_z - \mu] \begin{pmatrix}\psi_{R\uparrow}\\ \psi_{L\downarrow}\end{pmatrix}, \tag{2}$$

where $p_x = -i\hbar\partial_x$ and μ denotes the chemical potential. The presence of the ferromagnetic domain is accounted for by the term

$$H_Z = \int dx\, (\psi^\dagger_{R\uparrow},\psi^\dagger_{L\downarrow})\,\mathbf{m}(x)\cdot\boldsymbol{\sigma} \begin{pmatrix}\psi_{R\uparrow}\\ \psi_{L\downarrow}\end{pmatrix}, \tag{3}$$

where $\boldsymbol{\sigma} = (\sigma_x,\sigma_y,\sigma_z)$ are the Pauli matrices and $\mathbf{m}(x) = (m_\parallel \cos\phi, m_\parallel \sin\phi, m_z)$ is the space-dependent magnetization vector with $m_\parallel(x) > 0$. Here $m_\parallel(x)$ and $\phi(x)$ denotes the local absolute value and angle of the in-plane magnetization, respectively, and m_z the perpendicular magnetization component. The electron field operator $\psi^\dagger_{R\uparrow}(x)$ $[\psi_{R\uparrow}(x)]$ creates [annihilates] a right mover with spin $\uparrow$, while $\psi^\dagger_{L\downarrow}(x)$ $[\psi_{L\downarrow}(x)]$ creates [annihilates] a left mover with spin $\downarrow$. Finally, the superconducting pairing potential is given by

$$H_\Delta = \int dx\, [\Delta(x)\, \psi^\dagger_{R\uparrow}\psi^\dagger_{L\downarrow} + \Delta^*(x)\psi_{L\downarrow}\psi_{R\uparrow}]. \tag{4}$$

The Hamiltonian (1) can be rewritten in a Bogoliubov-de Gennes (BdG) form

$$H = \frac{1}{2}\int dx\, \Psi^\dagger \mathcal{H}_{\rm BdG}\Psi \tag{5}$$

by introducing the Nambu spinor $\Psi^\dagger = (\psi^\dagger_{R\uparrow},\psi^\dagger_{L\downarrow},\psi_{L\downarrow}, -\psi_{R\uparrow})$ and the Hamiltonian matrix

$$\mathcal{H}_{\rm BdG} = \begin{pmatrix} H_0^e & \Delta\sigma_0 \\ \Delta^*\sigma_0 & H_0^h\end{pmatrix}. \tag{6}$$

In Eq. (6),

$$H_0^e = v_F\sigma_z p_x - \mu\sigma_0 + \mathbf{m}(x)\cdot\boldsymbol{\sigma}, \tag{7a}$$

$$H_0^h = -\mathcal{T} H_0^e \mathcal{T}^{-1} = -\sigma_y \left(H_0^e\right)^* \sigma_y$$
$$= -v_F\sigma_z p_x + \mu\sigma_0 + \mathbf{m}(x)\cdot\boldsymbol{\sigma}, \tag{7b}$$

are the particle and hole sector diagonal blocks, respectively, σ_0 denotes the identity matrix in spin space [34], and $\mathcal{T} = \mathcal{K} i\sigma_y$ is the time-reversal operator, with $\mathcal{K}$ the complex conjugation.

For the moment, we keep an arbitrary profile for both the pairing potential $\Delta(x)$ and the ferromagnetic coupling $\mathbf{m}(x)$. Later, we specify $\Delta(x)$ for the case of N-S and S-N-S junctions, whereas general results will be given for an arbitrary profile $\mathbf{m}(x)$.

B. Quasiparticle states

The Hamiltonian (5) can be written in a diagonal form,

$$H = \sum_{\varepsilon_n \geqslant 0}\sum_j \varepsilon_n\, \gamma^\dagger_{\varepsilon_n,j}\gamma_{\varepsilon_n,j}, \tag{8}$$

where $\gamma^\dagger_{\varepsilon_n,j}$ and $\gamma_{\varepsilon_n,j}$, respectively, create and annihilate a fermionic quasiparticle with positive excitation energy ε_n, with respect to a ground state, whose energy has been set to zero. The label j accounts for possible degeneracies, examples of which are given in later sections. The diagonalization (8) is achieved from (5) through the ansatz

$$\Psi(x) = \sum_{\varepsilon_n \geqslant 0} \sum_j \{\varphi_{\varepsilon_n,j}(x)\gamma_{\varepsilon_n,j} + [\mathcal{C}\varphi_{\varepsilon_n,j}](x)\gamma^\dagger_{\varepsilon_n,j}\}, \tag{9}$$

where

$$\varphi_{\varepsilon_n,j} \doteq (u_{\varepsilon_n,j,\uparrow}, u_{\varepsilon_n,j,\downarrow}, v_{\varepsilon_n,j,\downarrow}, v_{\varepsilon_n,j,\uparrow})^T \tag{10}$$

is a solution of the BdG equation [35],

$$\mathcal{H}_{\rm BdG}\,\varphi_{\varepsilon_n,j} = \varepsilon_n \varphi_{\varepsilon_n,j}, \tag{11}$$

and $\mathcal{C}\varphi_{\varepsilon_n,j}$ is its charge-conjugated wave function. Here we have introduced the antiunitary charge-conjugation operator $\mathcal{C} = \mathcal{K}U_C$, with $U_C = \tau_y \otimes \sigma_y$, and $\mathcal{K}$ the complex conjugation. The relations (9) can be inverted, and the quasiparticle operator $\gamma_{\varepsilon_n,j}$ expressed as

$$\begin{aligned}\gamma_{\varepsilon_n,j} &= \int dx\,[\varphi^*_{\varepsilon_n,j}(x)]^T\,\Psi(x)\\ &= \int dx\,[u^*_{\varepsilon_n,j,\uparrow}(x)\psi_{R\uparrow}(x) + u^*_{\varepsilon_n,j,\downarrow}(x)\psi_{L\downarrow}(x)\\ &\quad + v^*_{\varepsilon_n,j,\downarrow}(x)\psi^\dagger_{L\downarrow}(x) - v^*_{\varepsilon_n,j,\uparrow}(x)\psi^\dagger_{R\uparrow}(x)],\end{aligned} \tag{12}$$

As can be seen from Eq. (6), in Eq. (11) the superconducting pairing potential couples a right- (left-) moving electron $u_{\varepsilon_n,j,\uparrow}$ ($u_{\varepsilon_n,j,\downarrow}$) to a left- (right-) moving hole $v_{\varepsilon_n,j,\downarrow}$ ($v_{\varepsilon_n,j,\uparrow}$). Furthermore, while the m_z component of the magnetization of the ferromagnetic domain preserves spin as a good quantum number, the in-plane magnetization $m_\parallel$ couples the dynamics of right- and left-moving electrons (holes), $u_{\varepsilon_n,j,\uparrow}$ ($v_{\varepsilon_n,j,\uparrow}$) and $u_{\varepsilon_n,j,\downarrow}$ ($v_{\varepsilon_n,j,\downarrow}$). Thus, differently from the standard treatment of FS junctions, where only the m_z magnetization is considered (see, e.g., Refs. [36–38]), no decoupling of the BdG equations into two 2×2 independent blocks occurs here, and the solutions of the BdG equations are always four-component wave functions $\varphi_{\varepsilon_n,j}$. The problem is therefore closer to that of hybrid structures with spin-orbit coupling, with the important difference that the ferromagnetic coupling does break time-reversal symmetry [39,40].

C. Particle-hole symmetry and Majorana states

It is well known that the BdG Hamiltonian (6) exhibits a built-in particle-hole symmetry. Indeed, one has $\mathcal{C}\mathcal{H}_{\rm BdG}\mathcal{C}^{-1} = U_C^\dagger \mathcal{H}^*_{\rm BdG} U_C = -\mathcal{H}_{\rm BdG}$. The particle-hole symmetry entails that, if $\varphi_{\varepsilon_n,j}$ is an eigenstate of $\mathcal{H}_{\rm BdG}$ with energy ε_n, then the charge-conjugated state, $\mathcal{C}\varphi_{\varepsilon_n,j}$, is an eigenstate of $\mathcal{H}_{\rm BdG}$ with energy $-\varepsilon_n$. Introducing the notation $\mathcal{C}\varphi_{\varepsilon_n,j} = \varphi_{-\varepsilon_n,j^c}$, the relation between components of charge-conjugated states reads

$$\begin{aligned}\varphi_{-\varepsilon_n,j^c} &= (u_{-\varepsilon_n,j^c,\uparrow}, u_{-\varepsilon_n,j^c,\downarrow}, v_{-\varepsilon_n,j^c,\downarrow}, v_{-\varepsilon_n,j^c,\uparrow})\\ &= \mathcal{C}\varphi_{\varepsilon_n,j} = (-v^*_{\varepsilon_n,j,\uparrow}, v^*_{\varepsilon_n,j,\downarrow}, u^*_{\varepsilon_n,j,\downarrow}, -u^*_{\varepsilon_n,j,\uparrow}),\end{aligned} \tag{13}$$

and, combining Eqs. (13) and (12), one obtains

$$\gamma^\dagger_{\varepsilon_n,j} = \gamma_{-\varepsilon_n,j^c}. \tag{14}$$

The latter allows for the potential existence of Majorana fermions, quasiparticles that are equal to their antiparticles ($\gamma^\dagger = \gamma$). Indeed, from Eq. (14) a quasiparticle excitation is a Majorana fermion if—and only if—it fulfills *two* conditions; namely, it (i) has vanishing energy and (ii) is invariant under charge conjugation, $j^c = j$. These conditions amount to state that a Majorana wave function $\varphi(x)$ is a kernel solution of the BdG equations, $\mathcal{H}_{\rm BdG}\,\varphi = 0$, that fulfills the constraint $\mathcal{C}\varphi = \varphi$; that is,

$$\begin{aligned}u_\uparrow &= -v^*_\uparrow,\\ u_\downarrow &= v^*_\downarrow.\end{aligned} \tag{15}$$

Any zero-energy fermionic quasiparticle $\gamma_{0,j}$ that is not Majorana-like ($j \neq j^c$) can always be decomposed as $\gamma_{0,j} = c_+ + ic_-$, where $c_+ \doteq \gamma_{0,j} + \gamma_{0,j^c}$ and $c_- \doteq -i\gamma_{0,j} + i\gamma_{0,j^c}$ are two Majorana fermions ($c_\pm = c_\pm^\dagger$). Because $c_\pm$ are linear combinations of quasiparticles within the same energy subspace, they are also proper excitations of the system. The corresponding Majorana wave functions are $\varphi_+ = \varphi_{0,j} + \varphi_{0,j^c}$ and $\varphi_- = -i\varphi_{0,j} + i\varphi_{0,j^c}$. Being zero-energy states, they are likely to be bound in regions of space where the superconducting gap closes, and, in certain situations, even spatially separated. In the next sections, we clarify the conditions of emergence of such MBSs in hybrid structures based on helical liquids and provide their explicit expressions in some relevant cases. We also notice that, formally, Majorana fermions can be constructed out of any pair of charge-conjugated fermionic quasiparticles $\gamma_{\varepsilon_n,j}$ and $\gamma_{-\varepsilon_n,j^c}$ of finite energy $\varepsilon_n > 0$. Indeed, taking two complex numbers α_+ and α_- such that $\alpha_+\alpha_-^* - \alpha_+^*\alpha_- \neq 0$, one can define two linearly independent, although not necessarily orthogonal, Majorana operators $c_\pm = \alpha_\pm\gamma_{\varepsilon_n,j} + \alpha_\pm^*\gamma_{-\varepsilon_n,j^c}$. Again, due to Eq. (14) one has $c_\pm = c_\pm^\dagger$. However, for $\varepsilon_n \neq 0$, such Majorana particles are not proper excitations of the system, as they are built up out of quasiparticles with opposite energies. The related wave functions are not stationary states of the BdG equations. A comprehensive discussion of the Majorana nature of Bogoliubov particles in superconductors is given by Chamon *et al.* in Ref. [41].

III. N-S JUNCTIONS

In this section, we study an N-S junction in the presence of an arbitrary ferromagnetic domain. Using a scattering theory approach, we derive a generic expression for the Andreev reflection probability and investigate the somewhat exotic case of a ferromagnetic dot.

A. A condition for perfect Andreev reflection

We start with considering the case of an interface between the helical state and one superconductor, as depicted in Fig. 1(a). Helicity forbids normal scattering at the N-S interface and, as a consequence, in the normal region N_2 an electron (a hole) is perfectly Andreev reflected as a hole (an electron) at any subgap excitation energy $\varepsilon < \Delta_0$ [42]. On the other hand, a ferromagnetic (F) region, as shown in Fig. 1, can induce normal backscattering. Let us first focus on this effect: An arbitrary F domain can be described in terms of a 2×2 unitary scattering matrix, which can be written in a polar representation (all symmetries are broken),

$$S_0^e(\varepsilon) = \begin{pmatrix} r_e(\varepsilon) & t'_e(\varepsilon) \\ t_e(\varepsilon) & r'_e(\varepsilon) \end{pmatrix} = e^{i\Gamma_m(\varepsilon)} \begin{pmatrix} -i\, e^{+i\Phi_m(\varepsilon)}\sqrt{1-T_\varepsilon} & e^{i\chi_m(\varepsilon)}\sqrt{T_\varepsilon} \\ e^{-i\chi_m(\varepsilon)}\sqrt{T_\varepsilon} & -i\, e^{-i\Phi_m(\varepsilon)}\sqrt{1-T_\varepsilon} \end{pmatrix}, \tag{16}$$

where $T_\varepsilon = |t_e(\varepsilon)|^2$ is the transmission coefficient of the F domain at excitation energy ε. The scattering matrix relates scattering amplitudes b's, for outgoing electrons in regions N_1 and N_2, to the incoming scattering amplitudes a's, according to $(b_{e,1},b_{e,2})^T = S_0^e(\varepsilon)(a_{e,1},a_{e,2})^T$. Based on specific realizations, some of which are further discussed below, one can ascribe a physical meaning to the other parameters as well. Indeed, $\Gamma_m \sim k_F L_m$ and $\Phi_m \sim k_F x_0$ (with $k_F = \mu/\hbar v_F$) are dynamical phases related to the spatial extension L_m of the F domain and to the location x_0 of its center with respect to the origin, respectively, whereas $\chi_m \sim m_z L_m$ is the relative phase shift between spin-↑ and spin-↓ electrons, accumulated along the domain due to the Zeeman coupling in the z direction. As far as the F domain is concerned, scattering of electrons and holes are decoupled. The scattering matrix for holes is easily obtained from Eq. (16), by noticing that if $u(\varepsilon)$ is a solution of $H_0^e u(\varepsilon) = \varepsilon u(\varepsilon)$, in the electron sector, then $v(\varepsilon) = i\sigma_y u(-\varepsilon)$ is a solution $H_0^h v(\varepsilon) = \varepsilon v(\varepsilon)$, in the hole sector. From this one can deduce the important relation [43]

$$S_0^h(\varepsilon) = -\sigma_z\, S_0^{e*}(-\varepsilon)\,\sigma_z. \tag{17}$$

The whole scattering matrix $S_N(\varepsilon) = \mathrm{Diag}[S_0^e(\varepsilon),S_0^h(\varepsilon)]$ now relates the outgoing scattering amplitudes b's, for electrons and holes in regions N_1 and N_2, to the incoming scattering amplitudes a's,

$$(b_{e,1},b_{e,2},b_{h,1},b_{h,2})^T = S_N(\varepsilon)(a_{e,1},a_{e,2},a_{h,1},a_{h,2})^T. \tag{18}$$

One has to combine such normal scattering with the Andreev scattering at the interface, which couples electrons and holes. For subgap excitation energies, perfect Andreev reflection at the N-S interface relates electron and hole scattering amplitudes in region N_2 through

$$\begin{pmatrix} a_{e,2} \\ a_{h,2} \end{pmatrix} = \alpha(E) \begin{pmatrix} 0 & e^{i\chi_R} \\ e^{-i\chi_R} & 0 \end{pmatrix} \begin{pmatrix} b_{e,2} \\ b_{h,2} \end{pmatrix}, \tag{19}$$

with $\alpha(\varepsilon) = \exp[-i\arccos(\varepsilon/\Delta_0)]$. Here we have assumed that the origin of the x axis is at the interface, as customary for the case of a N-S junction (for the S-N-S case there are two interfaces and a different choice is more suitable, as we shall see). Simple algebra leads to the reflection matrix, relating electron and hole amplitudes in region N_1 as

$$\begin{pmatrix} b_{e,1} \\ b_{h,1} \end{pmatrix} = \begin{pmatrix} r_{ee} & r_{eh} \\ r_{he} & r_{hh} \end{pmatrix} \begin{pmatrix} a_{e,1} \\ a_{h,1} \end{pmatrix}, \tag{20}$$

with

$$\begin{aligned} r_{ee} &= \frac{r_e - \alpha^2 r'_h \det S_0^e}{1-\alpha^2 r'_e r'_h}, \quad r_{eh} = \frac{\alpha\, t'_e t_h\, e^{i\chi_R}}{1-\alpha^2 r'_e r'_h}, \\ r_{he} &= \frac{\alpha\, t_e t'_h\, e^{-i\chi_R}}{1-\alpha^2 r'_e r'_h}, \quad r_{hh} = \frac{r_h - \alpha^2 r'_e \det S_0^h}{1-\alpha^2 r'_e r'_h}. \end{aligned} \tag{21}$$

It follows that $|r_{ee}|^2 = |r_{hh}|^2 \equiv R_N$, $|r_{eh}|^2 = |r_{he}|^2 \equiv R_A$, and $R_N + R_A = 1$, the latter relation reflecting current conservation. Notice that Eq. (20) entails that, for the N-S junction, for each eigenvalue ε of the BdG equation, there are two degenerate states [$j = 1,2$ in Eq. (8)], corresponding to the injection of an electron and the injection of a hole, respectively, from region N_1 [see Fig. 1(a)]. Using Eqs. (16) and (17) we arrive at the following general expression for the Andreev reflection probability at an N-S interface in a helical liquid,

$$R_A(\varepsilon) = \frac{T_\varepsilon\, T_{-\varepsilon}}{(1-\sqrt{R_\varepsilon R_{-\varepsilon}}\,)^2 + 4\cos^2\left[\arccos\frac{\varepsilon}{\Delta_0} + \Phi_m^A(\varepsilon)\right]\sqrt{R_\varepsilon R_{-\varepsilon}}}, \tag{22}$$

where $R_\varepsilon = 1 - T_\varepsilon$ is the reflection coefficient of the F domain and $\Phi_m^A(\varepsilon) = [\Phi_m(\varepsilon) - \Phi_m(-\varepsilon)]/2$ is an odd function of the energy ε that is extracted from the scattering matrix (16). One immediately sees from Eq. (22) that, independently of the parameters $\Phi_m^A(\varepsilon)$ and T_ε of the F region, $R_A(\varepsilon = 0) = 1$: The zero-energy mode is always perfectly Andreev reflected in a hybrid structure based on helical liquids.

Two comments are in order now. First, this result is quite different from the case of conventional N-S junctions, where backscattering can be induced also by non-F impurities leading to $R_A(\varepsilon = 0) = T_0^2/(2 - T_0)^2$ [44]. It is worth noticing that the difference in the result originates in Eq. (17), which leads to a minus sign in front of the first square root in the denominator of Eq. (22). The second comment is that, interestingly, the condition $R_A = 1$ of perfect Andreev reflection can, in principle, be satisfied by other, nonzero, energy modes as well. Indeed, the resonance condition for the F region to effectively become transparent is

$$(\sqrt{R_\varepsilon} - \sqrt{R_{-\varepsilon}})^2 + 4\cos^2\left[\arccos\frac{\varepsilon}{\Delta_0} + \Phi_m^A(\varepsilon)\right]\sqrt{R_\varepsilon R_{-\varepsilon}} = 0. \tag{23}$$

The resonances following from by Eq. (23) can be interpreted by considering the elementary process of an electron wave emerging from the F scatterer: After being converted into a counterpropagating hole at the N-S interface, it is backscattered again off the F scatterer, converted back to an electron at the N-S interface, and eventually impinges again onto the F domain. The phase accumulated along such a double-tour path causes, for certain energies, a constructive interference similar to the case of a Fabry-Perot interferometer. Equation (23) can thus be interpreted as the condition for Fabry-Perot resonances. Notice, however, that in this case the F domain plays the role of both mirrors of the resonator, and the length of the cavity of the resonator is effectively doubled due to the two Andreev reflections at the N-S interface. Furthermore, because of the electron-hole conversion, both the transmission for electrons (T_ε) and holes ($T_{-\varepsilon}$) appear in Eq. (23), as well as the phase shift $\arccos(\varepsilon/\Delta_0)$.

In order to illustrate the effect of the above general result, we consider as a first simple example the case depicted in Fig. 2(a) of one single F barrier located between x_1 and x_2,

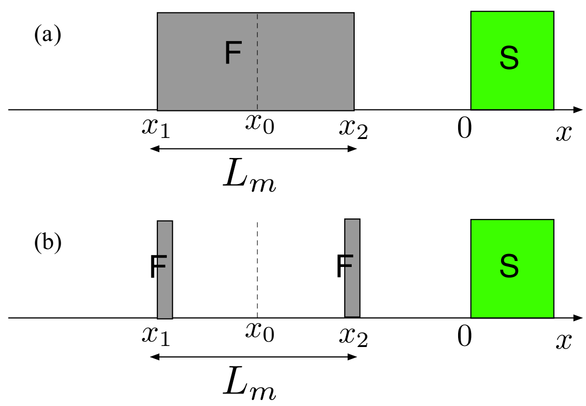

FIG. 2. (Color online) N-S junction with (a) a F barrier and (b) two ferromagnetic impurities, determining a ferromagnetic quantum dot.

characterized by a uniform magnetization,

$$\mathbf{m}(x) = \begin{cases} (m_\parallel \cos\phi, m_\parallel \sin\phi, m_z) & \text{if } x_1 \leqslant x \leqslant x_2, \\ 0 & \text{else.} \end{cases}$$

In this case, the parameters of the scattering matrix (16) acquire the following expressions. The phase Γ_m reads

$$\Gamma_m(\varepsilon) = \arctan[X(\varepsilon)] - \frac{(\mu+\varepsilon)L_m}{\hbar v_F}, \tag{24}$$

with

$$X(\varepsilon) = \begin{cases} \frac{(\mu+E)\tanh[\frac{L_m}{\hbar v_F}\sqrt{m_{||}^2-(\mu+E)^2}]}{\sqrt{m_{||}^2-(\mu+E)^2}}, & |\mu+\varepsilon| < m_{||}, \\ \frac{(\mu+E)\tan[\frac{L_m}{\hbar v_F}\sqrt{(\mu+E)^2-m_{||}^2}]}{\sqrt{(\mu+E)^2-m_{||}^2}}, & |\mu+\varepsilon| > m_{||}, \end{cases} \tag{25}$$

and $L_m = x_2 - x_1$ denoting the length of the barrier. The transmission coefficient reads

$$T_\varepsilon = \left(1 + Y_\varepsilon^2\right)^{-1}, \tag{26}$$

with

$$Y_\varepsilon = \begin{cases} \frac{m_{||}\sinh[\frac{L_m}{\hbar v_F}\sqrt{m_{||}^2-(\mu+\varepsilon)^2}]}{\sqrt{m_{||}^2-(\mu+\varepsilon)^2}}, & |\mu+\varepsilon| < m_{||}, \\ \frac{m_{||}\sin[\frac{L_m}{\hbar v_F}\sqrt{(\mu+\varepsilon)^2-m_{||}^2}]}{\sqrt{(\mu+\varepsilon)^2-m_{||}^2}}, & |\mu+\varepsilon| > m_{||}, \end{cases} \tag{27}$$

whereas $\chi_m(\varepsilon) \equiv \chi_z = m_z L_m/\hbar v_F$, $\Phi_m(\varepsilon) = 2x_0(\mu+\varepsilon)/\hbar v_F + \phi$, with $x_0 = (x_1+x_2)/2$ denoting the center of the barrier, implying $\Phi_m^A(\varepsilon) = 2\varepsilon x_0/\hbar v_F$ in Eqs. (22) and (23). Notice that, at the Dirac point, $\mu = 0$, $T_\varepsilon = T_{-\varepsilon}$, and Eq. (23) reduces to

$$\cos^2\left[\arccos\frac{\varepsilon}{\Delta_0} + \frac{2\varepsilon x_0}{\hbar v_F}\right](1 - T_\varepsilon) = 0. \tag{28}$$

As $T_\varepsilon \neq 1$ for all excitation energies, the perfectly Andreev reflected modes are those for which the energy satisfies

$$2\arccos\frac{\varepsilon}{\Delta_0} + \frac{4\varepsilon x_0}{\hbar v_F} = \pi + 2n\pi, \tag{29}$$

with n an integer. The latter equation turns out to be the condition for bound states to appear between the superconducting interface at $x = 0$ and a virtual infinite F wall at $x = x_0$. Indeed, the very same condition (29) is obtained also for $\mu \neq 0$, precisely in the limit of a strong barrier $m_\parallel \gg |\mu + E|$, where $T_\varepsilon \simeq T_{-\varepsilon} \simeq \cosh^{-2}(L_m m_{||}/\hbar v_F)$. In these particular conditions the Andreev reflection peaks, interpreted above as Fabry-Perot resonances, can also be understood in terms of resonant tunneling into bound-states. Note that, for $\mu \neq 0$ and a finite barrier strength $m_{||}$, the resonances at finite energies are no longer perfect, as $T_\varepsilon \neq T_{-\varepsilon}$.

B. A case study: The ferromagnetic quantum dot

As an illustration of the generality of Eq. (22), we consider the case where the F region consists of two impurities located at x_1 and x_2, described as two barriers of size δ, as displayed in Fig. 2(b), which we call F quantum dot [45]. The center of the dot is located at $x_0 = (x_1 + x_2)/2$. The magnetic texture is then taken as

$$\mathbf{m}(x) = \begin{cases} (m_1\cos\phi_1, m_1\sin\phi_1, m_{z1}) & \text{if } x_{1-} \leqslant x \leqslant x_{1+}, \\ (m_2\cos\phi_2, m_2\sin\phi_2, m_{z2}) & \text{if } x_{2-} \leqslant x \leqslant x_{2+}, \\ 0 & \text{else,} \end{cases}$$

with $x_{1\pm} = x_1 \pm \delta/2$ and $x_{2\pm} = x_2 \pm \delta/2$. We are interested in the limit of sharp barriers, i.e., $\delta \to 0$ and $m_{1,2} \to \infty$, with keeping $\mu_1 = m_1\delta/(\hbar v_F)$ and $\mu_2 = m_2\delta/(\hbar v_F)$ fixed and finite. We restrict ourselves to the case of equal barriers, $\mu_1 = \mu_2 \equiv \mu_0$, which captures the main features of the scattering problem. Combining the scattering matrices of the two single barriers, one can straightforwardly obtain the transmission probability of the double barrier as

$$T_\varepsilon = \frac{1}{\cosh^2(2\mu_0) - \sin^2\left(k_\varepsilon^e L_m + \Delta\phi/2\right)\sinh^2(2\mu_0)}, \tag{30}$$

with $k_\varepsilon^e = (\varepsilon + \mu)/\hbar v_F$, the electron wave vector in the normal region, $L_m = x_2 - x_1$ and $\Delta\phi = \phi_2 - \phi_1$. It appears that, for a fixed value of L_m, the chemical potential and the phase difference play a similar role, that is, breaking the symmetry between the transmission of particles and holes. In order to simplify the analysis in the various examples below, we vary only μ, and take $\Delta\phi = 0$. One should also note that for $L_m = 0$ and $\Delta\phi = 0$, T_ε in Eq. (30) reduces to the transmission probability of a single impurity of strength $2\mu_0$, located at x_0 [compare with Eqs. (26) and (27)]. For completeness, we also provide here the other parameters of the quantum dot scattering matrix, namely,

$$\begin{aligned} \Gamma_m(\varepsilon) &= -\arctan\left[\frac{\sin\left(2k_\varepsilon^e L_m + \Delta\phi\right)\sinh^2\mu_0}{1 + 2\sinh^2\mu_0\cos^2\left(k_\varepsilon^e L_m + \Delta\phi/2\right)}\right], \\ \Phi_m(\varepsilon) &= 2k_\varepsilon^e x_0 + \phi_0, \quad \phi_0 = (\phi_1 + \phi_2)/2, \\ \chi_m(\varepsilon) &= \chi_{z1} + \chi_{z2}, \end{aligned} \tag{31}$$

with $\chi_{zi} = m_{zi}\delta/(\hbar v_F)$, which we keep finite as $\delta \to 0$.

In Figs. 3 and 4 we plot the Andreev reflection probability as a function of the excitation energy, for different values of the parameters. The various cases show that the zero mode is always perfectly Andreev reflected, consistent with Eq. (22). Right at the Dirac point, the modes satisfying the condition of Eq. (29) are perfectly Andreev reflected. We distinguish

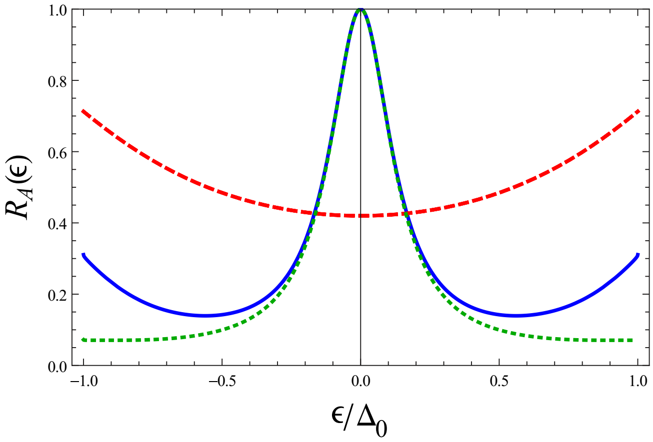

(a) $\mu_0 = 0.5, \mu = 0, L_m = 1, x_0 = 1.5, \Delta\phi = 0$

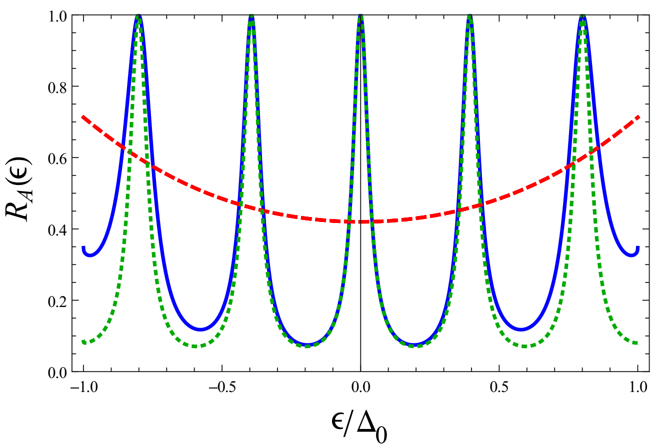

(b) $\mu_0 = 0.5, \mu = 0, L_m = 1, x_0 = 4.5, \Delta\phi = 0$

FIG. 3. (Color online) Influence of the position x_0 of the F region on the Andreev reflection probability in the double-barrier case (blue solid line). For a better interpretation, we also plotted the transmission probability T_ε and $T_{-\varepsilon}$ of the double barrier (red dashed line) and the Andreev reflection probability for a single impurity of strength $2\mu_0$ located at x_0 (green dotted line). Energies are given in units of Δ_0 and lengths in units of the superconductor coherence length $\hbar v_F/\Delta_0$.

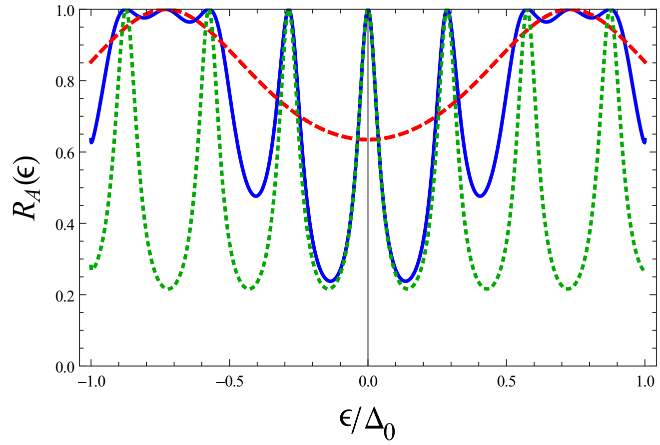

(a) $\mu_0 = 0.35, \mu = 0, L_m = 2.15, x_0 = 6$

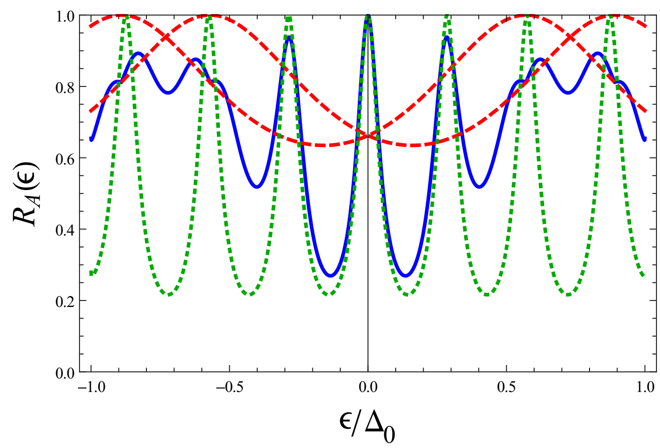

(b) $\mu_0 = 0.35, \mu = 0.16, L_m = 2.15, x_0 = 6$

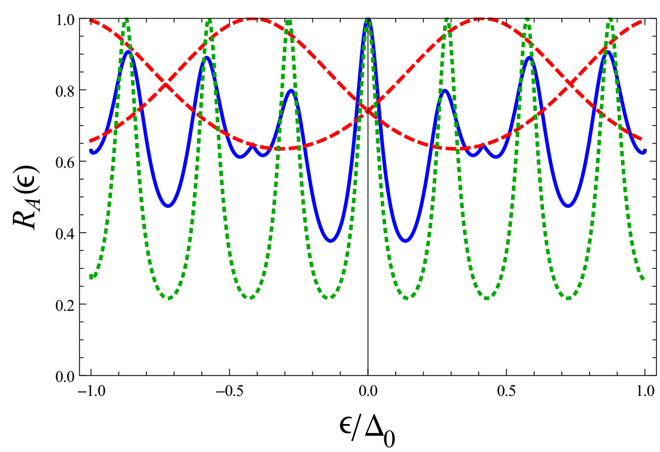

(c) $\mu_0 = 0.35, \mu = 0.3, L_m = 2.15, x_0 = 6$

FIG. 4. (Color online) Influence of the chemical potential μ on the Andreev reflection probability in the double-barrier case (blue solid line). In all three plots, $\Delta\phi = 0$. For a better interpretation, we also plotted the transmission probability T_ε and $T_{-\varepsilon}$ of the double barrier (red dashed line) and the Andreev reflection probability for a single impurity of strength $2\mu_0$ located in x_0 (green dotted line). Energies are given in units of Δ_0 and lengths in units of the superconductor coherence length $\hbar v_F/\Delta_0$.

two kinds of such modes. First, there are the Fabry-Pérot-like modes, whose energy satisfies the same Eq. (29) as for the single barrier case, with x_0 now the center of the F dot. The density of such modes increases with $|x_0|$, as illustrated in Figs. 3(a) and 3(b). Second, the modes for which $T_\varepsilon = 1$ are also perfectly Andreev reflected, a possibility that does not arise in the single barrier case. Generally speaking, as compared to a single impurity in x_0, $R_A(\varepsilon)$ is modulated by the transmission coefficient of the double-barrier structure. Varying the chemical potential ($\mu \neq 0$) leads to several interesting modifications. While the positions of the maxima corresponding to the virtual bound states are barely altered, their amplitude is no longer 1—they are not perfectly Andreev reflected anymore—except for the zero-energy mode, which remains pinned to 1. Furthermore, the peaks corresponding to the open channels of the dot now split, as T_ε and $T_{-\varepsilon}$ are no longer equal. This particular evolution as a function of the chemical potential is depicted in Figs. 4(a)–4(c).

We conclude this section with a comment about the difference between our results and the multipeak structure shown in Ref. [8]. There the surface of a 3D topological insulator in proximity to a superconductor and a ferromagnet gives rise to chiral 1D Majorana states. In contrast, in our lower-dimensional situation, 0D Majorana states appear. Furthermore, while the multipeak structure of Ref. [8] indicates the presence or absence of Majoranas and vortices, our multipeak structure provides information about the nature of the F barrier (acting on the helical liquid) and the resulting Fabry-Pérot resonance phenomena.

C. Majorana wave functions

In this section, we discuss the relation between perfect Andreev reflection and the presence of Majorana states. We come back to the somewhat simpler case of a single F barrier, for which the transmission probability is given in Eq. (26). As discussed before, the Andreev reflection probability can have many peaks as a function of energy, the positions and number of which depend on the location x_0 of the center of the barrier. However, except in the special situation $\mu = 0$, only the zero-energy mode is perfectly Andreev reflected. Such a robust peak is often interpreted in the context of topological superconductivity as the signature of tunneling into a MBS. Here the situation is more subtle, as there is no real bound state to begin with, contrary to the case of a genuine spinless p-wave superconductor.

The zero-energy states are always delocalized in the whole normal region that is ungapped. In the absence of a scattering region, Andreev reflection at the interface imposes that scattering states are superpositions of electron and hole components. The zero-energy subspace is 2D and spanned by two orthogonal eigenstates of the BdG Hamiltonian that are charge conjugated (we drop the label $\varepsilon = 0$ for simplicity). The first wave function φ_1 corresponds to injecting a Cooper pair in the superconductor (it is the superposition of a right-moving electron and a left-moving hole). The second wave function $\varphi_2 = \mathcal{C}\varphi_1$ is denoted by φ_{1^c}, according to the notation of Sec. II, and corresponds to the opposite process, the injection of a Cooper from the superconductor into the normal lead (it is the superposition of a left-moving electron and a right-moving hole). Their explicit expressions, in Nambu space, read

$$\varphi_1(x) = \begin{pmatrix} 1 \\ 0 \\ -i e^{-i\chi_R} \\ 0 \end{pmatrix} e^{ik_F x}, \quad \varphi_{1^c}(x) = \begin{pmatrix} 0 \\ i e^{i\chi_R} \\ 0 \\ -1 \end{pmatrix} e^{-ik_F x}. \quad (32)$$

If one imposes a hard-wall boundary condition in the form of an infinite F barrier, somewhere in the normal region, then the only allowed solution is a superposition of φ_1 and φ_{1^c} that is indeed a single Majorana state. This assumption connects the present situation to the nanowire setups where such a hard-wall boundary is usually imposed [16]. If one removes the hard wall, then there are not one but two independent Majorana states, being linear combinations of φ_1 and φ_{1^c}. It turns out that a F barrier, as depicted in Fig. 2(a) can localize the two Majorana states on either side of the barrier. In order to prove this statement, we first compute the scattering states at zero energy in the presence of the barrier. Their wave functions are given in the Appendix and coincide in the region $x < x_1$ with the states of Eq. (32). Following the general scheme of Majorana states given in Sec. II, we construct two independent Majorana wave functions, $\varphi_+^{\rm NS}$ and $\varphi_-^{\rm NS}$, given by $\varphi_\pm^{\rm NS} = \alpha_\pm\varphi_1 + \alpha_\pm^*\varphi_{1^c}$. A suitable choice of $\alpha_\pm$—given in the Appendix —leads $\varphi_\pm^{\rm NS}$ to acquire the simple form

$$\varphi_\eta^{\rm NS}(x) = \begin{pmatrix} f_\eta(x)\, e^{\frac{i}{2}[\frac{\pi}{2}+\chi_R-\int_0^x \frac{2m_z(x')}{\hbar v_F}dx']} \\ f_\eta^*(x)\, e^{\frac{i}{2}[\frac{\pi}{2}+\chi_R-\int_0^x \frac{2m_z(x')}{\hbar v_F}dx']} \\ f_\eta(x)\, e^{-\frac{i}{2}[\frac{\pi}{2}+\chi_R-\int_0^x \frac{2m_z(x')}{\hbar v_F}dx']} \\ -f_\eta^*(x)\, e^{-\frac{i}{2}[\frac{\pi}{2}+\chi_R-\int_0^x \frac{2m_z(x')}{\hbar v_F}dx']} \end{pmatrix}, \quad (33)$$

with $\eta = \pm$,

$$f_\eta(x) = \frac{e^{-i\frac{\phi+\eta\tilde\theta_0}{2}}}{2\cosh\frac{\kappa L_m}{2}} \begin{cases} e^{ik_F(x-x_1)}\, e^{-\eta\frac{\kappa L_m}{2}}, & x \leqslant x_1, \\ e^{\eta\kappa(x-x_0)}, & x_1 \leqslant x \leqslant x_2, \\ e^{ik_F(x-x_1)}\, e^{\eta\frac{\kappa L_m}{2}}, & x \geqslant x_2, \end{cases} \quad (34)$$

and $\kappa = \sqrt{m_\parallel^2 - \mu^2}/\hbar v_F$, $k_F = \mu/\hbar v_F$, $\tilde\theta_0 = \arccos(\mu/m_\parallel)$, $\mu < m_\parallel$. One can easily check that the $\varphi_{\eta=\pm}^{\rm NS}$ are indeed invariant under charge conjugation; that is, $\mathcal{C}\varphi_\pm^{\rm NS} = \varphi_\pm^{\rm NS}$, with $\mathcal{C} = \mathcal{K}\,\tau_y \otimes \sigma_y$. Note that the two wave functions have opposite exponential variations inside the F region $x_1 \leqslant x \leqslant x_2$. Although both Majorana states are extended over the whole normal region, they are still spatially localized on opposite sides of the F domain, as drawn schematically in Fig. 5. In contrast, the zero-energy Andreev states φ_1 and φ_{1^c} are mixtures of these two wave functions and hence cannot be considered as localized in any meaningful way. The situation is quite similar to the case of a Schrödinger particle in one dimension. At a given energy two scattering states, namely, a right-moving and a left-moving plane wave, are present. Confining the particle in a box reduces the number of states, from two plane waves to one bound state, at given quantized energies. However, putting the particle on a ring (or enforcing periodic boundary conditions), although it quantizes the energy, does not reduce the number of states, and one is again left with one left mover and one right mover. Interestingly, in the context of hybrid structures, such

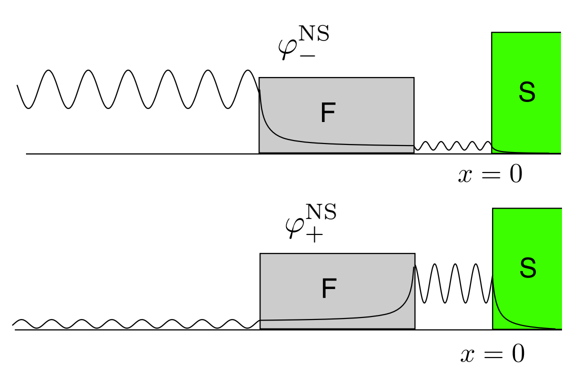

FIG. 5. (Color online) Sketch of two Majorana states, at $\varepsilon = 0$, in the presence of a F barrier. Even though they do extend on the whole normal region, they are predominantly localized on one side or the other of the F domain (see text).

periodic boundary conditions are effectively achieved by adding a second superconducting electrode to the previous setup, therefore creating an S-N-S junction [46,47]. Indeed, we show in the next section that the two Majorana states are barely affected; they are by construction in an equal weight superposition of electron and hole and ready to be bound by a superconducting mirror.

IV. S-N-S (JOSEPHSON) JUNCTIONS

In this section, we study a Josephson junction in the presence of an arbitrary F domain. Using the same scattering approach as in Sec. III, we derive a generic expression for the Andreev bound-state condition and investigate the evolution of the spectrum in the presence of a F dot.

A. Andreev bound states and Josephson current

We now turn our attention to the case of S-N-S junctions with an arbitrary F domain in the normal region. Aiming at drawing analogies with the former case of the N-S junction, we focus on subgap transport and start by deriving the condition for Andreev bound states [48]. We can use most of the results of the previous section. Scattering amplitudes in region N_2 are still connected by the electron and hole scattering matrices as in Eq. (18). One only needs to implement a similar condition for perfect Andreev reflection in region N_1. Moreover, for the S-N-S case it is more convenient to set the origin at the center of the junction, so that the two interfaces are located at $x = \pm L/2$, with L denoting the interface distance. The whole Andreev reflection process at both interfaces can be written in terms of scattering amplitudes as

$$(a_{e,1},a_{e,2},a_{h,1},a_{h,2})^T = S_A(\varepsilon)(b_{e,1},b_{e,2},b_{h,1},b_{h,2})^T, \quad (35)$$

with

$$S_A(\varepsilon) = \begin{pmatrix} 0 & \alpha'(\varepsilon)\mathsf{r}_A \\ \alpha'(\varepsilon)\mathsf{r}_A^* & 0 \end{pmatrix} \quad (36)$$

denoting a 4×4 matrix where $\alpha'(\varepsilon) = \exp[-i\arccos(\varepsilon/\Delta_0) + i(k_\varepsilon^e - k_\varepsilon^h)L]$ and $\mathsf{r}_A = \mathrm{Diag}[e^{i\chi/2},e^{-i\chi/2}]$. In the case of a helical liquid with a linear spectrum, $k_\varepsilon^{e/h} = (\mu \pm E)/\hbar v_F$ and we simply have $k_\varepsilon^e - k_\varepsilon^h = 2\varepsilon/\hbar v_F$. Combining Eq. (18) and (35), we arrive at the well-known compatibility condition [49]

$$\det[\tau_0 \otimes \sigma_0 - S_A(\varepsilon)\, S_N(\varepsilon)] = 0, \quad (37)$$

for the Andreev bound states (ABSs). In our case, the latter equation acquires the simple form

$$\cos^2\left\{\arccos\frac{\varepsilon}{\Delta_0} - \frac{\varepsilon\left[L-\lambda_m^S(\varepsilon)\right]}{\hbar v_F}\right\} = \frac{1}{2}\big\{1-\sqrt{R_\varepsilon R_{-\varepsilon}}\,\cos\left[2\Phi_m^A(\varepsilon)\right] + \sqrt{T_\varepsilon T_{-\varepsilon}}\,\cos\left[\chi - 2\chi_m^S(\varepsilon)\right]\big\}, \quad (38)$$

where the odd function of the energy $\Phi_m^A(\varepsilon) = [\Phi_m(\varepsilon) - \Phi_m(-\varepsilon)]/2$, as well as the even functions $\lambda_m^S(\varepsilon) = \hbar v_F[\Gamma_m(-\varepsilon) - \Gamma_m(\varepsilon)]/2\varepsilon$ and $\chi_m^S(\varepsilon) = [\chi_m(\varepsilon) + \chi_m(-\varepsilon)]/2$ are directly extracted from the scattering matrix (16) describing the F scatterer. Equation (38) thus determines the Andreev bound levels in the presence of an arbitrary F scatterer and represents another important result of the paper.

In order to illustrate its physical consequences, we exploit one enlightening example, namely, the case of a F quantum dot realized by two F barriers, as sketched in Fig. 6(a). The case of equal barriers captures the main physical ingredients of the problem and we restrict to this situation. The functions T_ε, $\Phi_m^A(\varepsilon)$, $\chi_m^S(\varepsilon)$, and $\lambda_m^S(\varepsilon)$ appearing in Eq. (38) are in this case straightforwardly obtained from the scattering matrix of the dot, given at the end of Sec. III A. In particular, Eq. (30) yields the transmission coefficient T_ε, whereas from Eq. (31) one obtains $\Phi_m^A(\varepsilon) = 2\varepsilon x_0/\hbar v_F$, $\chi_m^S(\varepsilon) \equiv \chi_z$, and $\lambda_m^S(\varepsilon)$ through $\Gamma_m(\varepsilon)$. The Andreev bound levels obtained from the solution of Eq. (38) are plotted in Figs. 6(c) and 6(d) as a function of the superconducting phase difference χ, for various values of the location x_0 of the quantum dot center and the chemical potential μ, respectively. The first emerging feature is that the levels are symmetric in energy with respect to $\varepsilon = 0$. This is due to the particle-hole symmetry of the BdG equations. Indeed, from the general properties of Eq. (38) one can easily check that, because $\Phi_m^A(\varepsilon)$ is odd and $\lambda_m^S(\varepsilon)$ and $\chi_m^S(\varepsilon)$ are even, if ε is a solution of Eq. (38), then $-\varepsilon$ is also a solution. Second, the plots are symmetric in the phase difference χ around the symmetry value $\chi - 2\chi_z = \pi$. Indeed, from Eq. (38) one can see that, if a bound state exists for a given energy at a value χ_1, another one necessarily exists at $\chi_2 = 2[\pi + \chi_m^S(\varepsilon)] - \chi_1$, so that there are two bound states in a 2π interval centered around $\chi - 2\chi_m^S(\varepsilon) = \pi$. The spectrum of Andreev bound levels is 2π periodic with the phase difference χ. However, the Andreev states do not necessarily have the same periodicity, as we discuss below. We notice also that the renormalization of the superconducting phase difference as $\chi \to \chi - 2\chi_z$ caused by the m_z magnetization induces a π junction behavior when $\chi_z \gtrsim \pi/2$. The third feature emerging from Fig. 6 is the existence of crossing points. To discuss their physical meaning, it is worth recalling that, differently from conventional S-N-S junctions, here for each value of $\chi - 2\chi_z$ the Andreev levels are typically nondegenerate, due to the helical nature of the edge states. Crossing points, however, are an exception and correspond to degenerate eigenvalues of the BdG equations. It is interesting to analyze whether the corresponding degenerate states hybridize or not. In Fig. 6(c), we show the evolution of the ABS spectrum with the position x_0 of the dot center at the Dirac point $\mu = 0$. In order to understand the pattern of gap openings, one must bear in mind the resonances in the dot transmission probability T_ε, plotted in Fig. 6(b). On Figs. 6(c) and 6(d), open and solid arrows indicate the ABSs that are close to open and closed channels of the dot, respectively. These have very different behaviors as x_0 is moved away from the center of the junction. Indeed, for open channels, $T_\varepsilon \simeq 1$ and $R_\varepsilon \simeq 0$, such that the condition for ABS barely depends on x_0, as one can see in Eq. (38). On the other hand, for closed channels, $T_\varepsilon \simeq 0$ and $R_\varepsilon \simeq 1$, and the condition for ABS barely depends on the phase difference anymore, which explains the flatness of the bands. Note that, although the zero mode is, in principle, a closed channel of the dot, it is unaffected by changes in the position. Tuning the chemical potential away from $\mu = 0$ also has the effect of opening gaps for all ABSs, as can be seen in Fig. 6(d). Again, the crossing point at $\varepsilon = 0$ is stably preserved. The crossing point at $\varepsilon = 0$ is thus the only

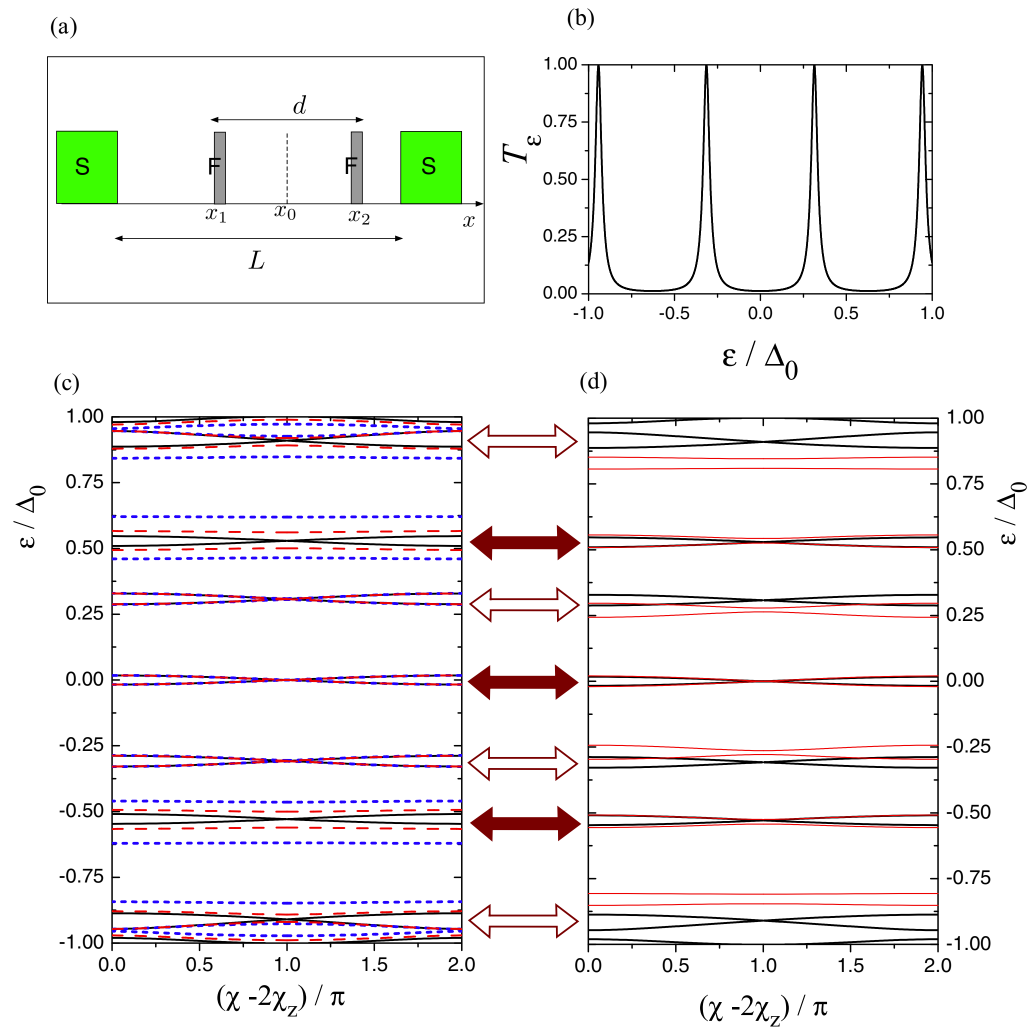

FIG. 6. (Color online) Andreev bound levels for the case of a F quantum dot. (a) Sketch of the realization of the system, where two F barriers are located inside the S-N-S junction of topological edge states. Here we have considered two δ-like barriers with the same strength parameter $\mu_0 = 1.44$ (corresponding to a transmission of 20% for each barrier), separated by a distance $d = L/2$, and with equal magnetizations ($\phi_1 = \phi_2 = 0$ and $m_{z1} = m_{z2} = m_z$). (b) The transmission coefficient T_ε of the dot, plotted as a function of energy for $\mu = 0$, shows resonances corresponding to the open channels of the quantum dot. (c) Andreev bound levels at the Dirac point ($\mu = 0$) are plotted as a function of the superconductor phase difference χ, in the case of a long junction ($L = 10\hbar v_F/\Delta_0$), for different values of the location of the dot center: $x_0/L = 0$ (solid black), $x_0/L = 0.02$ (dashed red), and $x_0/L = 0.05$ (dotted blue). (d) The Andreev bound levels for the case of a centered quantum dot ($x_0 = 0$) for different values of chemical potential: $\mu = 0$ (thick black) and $\mu = \Delta_0/2$ (thin red). Andreev levels appear not only around the resonances of the dot (denoted by open arrows) but also in correspondence with off-resonance energies (solid arrows). Only the level around $\varepsilon = 0$ is stable against variations of x_0 and μ and always carries a current.

one that is stable to any parameter variation. This is, in fact, a general feature that stems from Eq. (38), from which one can see that $\varepsilon = 0$ and $\chi - 2\chi_m^S(0) = \pi$ is always a solution of the ABS equation, in sharp contrast with conventional s-wave junctions, where normal backscattering opens a gap at zero energy. The crossing at zero energy is protected because the two Andreev states, being charge-conjugated to each other, have different fermion parities. Indeed, the Hamiltonian for the two states crossing zero energy can be written as

$$H_{\mathrm{ABS},0} = \tfrac{1}{2}\varepsilon_0(\chi)\Gamma_0^\dagger\Gamma_0 - \tfrac{1}{2}\varepsilon_0(\chi)\Gamma_{0^c}^\dagger\Gamma_{0^c}, \tag{39}$$

or, using $\Gamma_{0^c} = \Gamma_0^\dagger$ following from particle-hole symmetry [26],

$$H_{\mathrm{ABS},0} = \varepsilon_0(\chi)\left(\Gamma_0^\dagger\Gamma_0 - \tfrac{1}{2}\right) + \tfrac{1}{2}\varepsilon_0(\chi). \tag{40}$$

The two Andreev states, with energy $\pm\varepsilon_0(\chi)$ correspond to the two parity sectors, $\Gamma_0^\dagger\Gamma_0 = 0,1$. Such a protection directly affects the Josephson current. Indeed, ABSs carry a stationary supercurrent across the junction, as the two Andreev reflections have the effect of transferring a Cooper pair from one superconducting contact to the other one. At zero temperature, each ABS contributes $J_n = (e/h)\partial_\chi\varepsilon_n(\chi)$ to the total Josephson current. Levels with opposite energies therefore carry opposite supercurrents, as do degenerate levels on opposite sides of $\chi - 2\chi_m^S(\varepsilon) = \pi$. As a consequence of the protected crossing at the $\varepsilon = 0$ level, although the spectrum is 2π periodic, the Josephson current is only 4π periodic. Indeed, while higher-energy Andreev levels contribute a 2π periodic Josephson current, the current carried by this level is actually 4π periodic, a signature of the fermion parity anomaly in helical Josephson junctions [1,26,47]. Note that the 2π current can be considerably reduced, almost filtered out, by the presence of an off-centered quantum dot, as many high-energy levels become flat.

We conclude this section by observing that, for the case of a single barrier, analytic expressions for the ABS can be determined in the limit of strong in-plane magnetization $m_\parallel \gg \mu, |\varepsilon|$. Indeed, in this limit the transmission probability T_ε of the single barrier [see Eq. (26)] becomes energy independent and reduces to $T_\varepsilon \to T_\infty = 1/\cosh^2 \mu_0$, with $\mu_0 = m_\parallel L_m/\hbar v_F$ parametrizing the strength of the barrier, whereas the length scale λ_m^S reduces to $\lambda_m^S(\varepsilon) \to L_m$. In the special case of a barrier centered in the middle of the junction, $x_0 = 0$, and at $\chi - 2\chi_z = \pi$, the position of ABSs is simply given by

$$\frac{\varepsilon(L - L_m)}{\hbar v_F} - \arccos\frac{\varepsilon}{\Delta_0} = -\frac{\pi}{2} + m\,\pi, \tag{41}$$

which is the analog of the condition (29) for resonant states in the N-S junction. In this limit the positions of all these ABSs (not just the one at $\varepsilon = 0$) are insensitive to the strength μ_0 of the barrier. When $L_m = L$ we recover the limit studied by Fu and Kane in Ref. [26] and only the zero-energy mode is pinned. The other extreme limit of $L_m = 0$ corresponds to the impurity studied in Ref. [31]. Interestingly, the relevant length scale in the problem is $L - L_m$. Equation (41) shows that the condition for the definition of short and long junctions should actually be formulated in terms of the interface length $L - L_m$. The short junction limit would correspond to $L - L_m \ll \hbar v_F/\Delta_0$, while the long junction would correspond to $L - L_m \gg \hbar v_F/\Delta_0$. In particular, the density of ABSs will be set by the length $L - L_m$. In the short junction limit, one can also show that there are only two Andreev bound levels, given by

$$\varepsilon_\pm(\chi) = \pm\Delta_0\sqrt{T_0}\cos\left(\frac{\chi}{2} - \chi_z\right), \tag{42}$$

which show the 4π periodicity, in agreement with the results by Fu and Kane [26] and Kwon *et al.* [50]. This result should be compared with the short-junction limit for conventional S-N-S junctions, $\varepsilon_\pm(\chi) = \pm\Delta_0[1 - T_0\sin^2(\chi/2)]^{1/2}$, which is 2π periodic [49]. It is worth emphasizing that such a difference in the results stems from the minus sign in front of the $\sqrt{R_\varepsilon R_{-\varepsilon}}$ on the right-hand side of Eq. (38). Similarly to the case of the N-S junction, this sign is a consequence of Eq. (17).

B. Majorana wave functions

We close our analysis with a discussion of the Majorana wave-functions in the S-N-S case. A comparison with the N-S junction is quite enlightening here. We know from the latter case that, at zero energy, there are two charge-conjugated Andreev states corresponding to a right-moving electron being reflected as a left-moving hole and a right-moving hole being reflected as a left-moving electron. The extra superconducting electrode transforms these two extended Andreev states into ABSs, carrying opposite supercurrents. Again, one can decompose this single, zero-energy fermionic level into two Majorana wave-functions φ_+ and φ_- given by

$$\varphi^{\rm SNS}_{\eta=\pm}(x) = \begin{pmatrix} f_\eta(x)\, e^{-i\int_{x_0}^{x}\frac{m_z(x')}{\hbar v_F}dx'} \\ f_\eta^*(x)\, e^{-i\int_{x_0}^{x}\frac{m_z(x')}{\hbar v_F}dx'} \\ f_\eta(x)\, e^{+i\int_{x_0}^{x}\frac{m_z(x')}{\hbar v_F}dx'} \\ -f_\eta^*(x)\, e^{+i\int_{x_0}^{x}\frac{m_z(x')}{\hbar v_F}dx'} \end{pmatrix}, \tag{43}$$

in Nambu space, with

$$f_\eta(x) = \frac{e^{-i\frac{\phi+\eta\tilde\theta_0}{2}}}{2\cosh\frac{\kappa L_m}{2}}\begin{cases} e^{ik_F(x-x_1)}\,e^{-\eta\frac{\kappa L_m}{2}} & x \leqslant x_1, \\ e^{\eta\kappa(x-x_0)} & x_1 \leqslant x \leqslant x_2, \\ e^{ik_F(x-x_2)}\,e^{\eta\frac{\kappa L_m}{2}} & x \geqslant x_2, \end{cases} \tag{44}$$

and $\kappa = \sqrt{m_\parallel^2 - \mu^2}/\hbar v_F$, $\tilde\theta_0 = \arccos(\mu/m_\parallel)$, $\mu < m_\parallel$. Notice that the wave function $f_\eta(x)$, which depends on the *in-plane* magnetization $m_\parallel$, is the *same* for the S-N-S case [Eq. (44)] and for the N-S case [Eq. (34)]. The difference between $\varphi_\eta^{\rm NS}(x)$ in Eq. (33) and $\varphi_\eta^{\rm SNS}(x)$ in Eq. (43) lies in the other phase factors that arise from the phase difference across the junction and the m_z magnetization only. As in the N-S case, although extended in the whole normal region these wave functions are localized on opposite sides of the F domain (see Fig. 7 for a schematic illustration). The fact that two Majorana states arise in such a S-N-S junction can be contrasted with a similar situation in topological nanowire junctions. There again, two MBSs exist on their own at the edges of the superconductors. When a junction is formed, they simply delocalize in the whole normal region [15]. In the present case, helicity combined with fermion parity conservation protects the zero-energy crossing and allows for the appearance of Majorana states that can be localized by a F domain. What is more surprising is that one superconducting contact alone is able to *preform* such localized states.

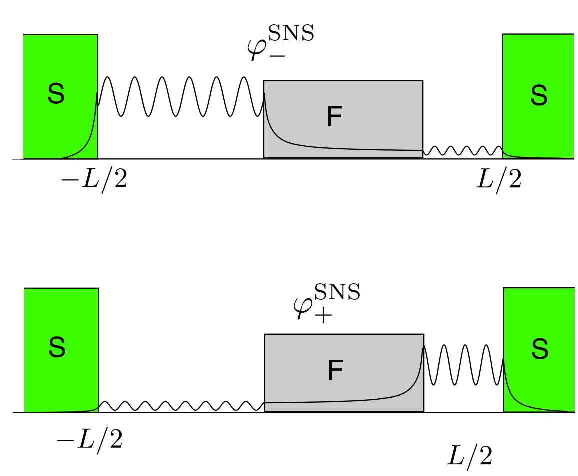

FIG. 7. (Color online) Sketch of the two Majorana states at $\varepsilon = 0$ and $\chi - 2\chi_s(0) = \pi$. Similar to the N-S case (see Fig. 5), even though they do extend on the whole normal region, they are predominantly localized on one side or the other of the F domain.

V. CONCLUSION

We have studied transport properties of hybrid structures based on helical liquids at the edge of a QSHI. We explicitly computed the Andreev reflection coefficient for N-S junctions and the condition for ABSs in S-N-S junctions, in both cases in the presence of an arbitrary F scatterer. We found that many peaks, and not only a zero-bias peak, arise in the conductance measurement of N-S junctions, due to Fabry-Pérot like resonances. The heights of these peaks depend on external, possibly controllable, parameters, like the chemical potential or the form of the F barrier. In particular, the response of the double-barrier setup, which we studied in detail, is very sensitive to the value of the chemical potential, which can, in principle, be controlled by an external gate. As the gate is varied, while some peaks change positions and height and others even split, the zero-bias peak remains pinned. This effect should provide an experimental test to probe the peculiar and very rich interplay of helicity and superconductivity at the edge of a topological insulator, as well as to single out evidence of the Majorana zero modes. We have also shown, by computing the wave functions, that the presence of a F domain already localizes two Majorana modes at the N-S interface. Adding a second superconducting contact binds them in a finite size S-N-S Josephson junction. There, the two Majorana states hybridize, forming an Andreev level. We have also analyzed the general structure of the ABSs spectrum, for an arbitrary F region. We found that the effective phase difference across the junction, as well as the effective length of the junction, are renormalized in an energy-dependent way by the scatterer, the latter leading to a redefinition of the short and long junction limits in the strong barrier case. Degenerate levels, manifested as crossing points in the spectrum at a phase difference of π, appear in the case of a barrier exactly centered in the junction. However, only the zero-energy crossing is truly protected due to fermion parity conservation, and, as a consequence, the Josephson current across the junction is 4π periodic, a hallmark of the edge-state helicity.

ACKNOWLEDGMENTS

We would like to acknowledge financial support by the DFG (German-Japanese research unit "Topotronics" and SPP 1666) as well as the Helmoltz Foundation (VITI). F.D. thanks the University of Würzburg for financial support and hospitality during his stay as a guest professor and also acknowledges FIRB 2012 project HybridNanoDev (Grant No. RBFR1236VV).

APPENDIX: WAVE FUNCTIONS IN THE ZERO-ENERGY SUBSPACE OF N-S JUNCTIONS

We present here the wave functions of the two zero-energy scattering states, in the case of the N-S junction with a single F barrier, as shown in Fig. 2(a). Since the zero-energy modes are perfectly Andreev reflected, in region $x < x_1$ the wave functions are either superpositions of an incoming electron and a reflected hole or an incoming electron and a reflected hole. The first four-component wave function, which we denote by $\varphi_1(x)$, corresponds to the injection of a Cooper pair in the superconductor and has the wave function

$$\varphi_1(x) = \begin{pmatrix} u_{\uparrow,1}(x) \\ u_{\downarrow,1}(x) \\ v_{\downarrow,1}(x) \\ v_{\uparrow,1}(x) \end{pmatrix} = \begin{cases} \begin{pmatrix} 1 \\ 0 \\ -ie^{-i(2\chi_z+\chi_R)} \\ 0 \end{pmatrix} e^{ik_F x} & x < x_1, \\ \begin{pmatrix} \frac{e^{-i\frac{m_z(x-x_0)}{\hbar v_F}} e^{-i\frac{\chi_z}{2}}}{2\sin\tilde{\theta}_0} i e^{ik_F x_1}[e^{\kappa(x-x_0)} e^{\frac{\kappa L_m}{2}} e^{-i\tilde{\theta}_0} - e^{-\kappa(x-x_0)} e^{-\frac{\kappa L_m}{2}} e^{i\tilde{\theta}_0}] \\ e^{i\phi} \frac{e^{-i\frac{m_z(x-x_0)}{\hbar v_F}} e^{-i\frac{\chi_z}{2}}}{2\sin\tilde{\theta}_0} i e^{ik_F x_1}[e^{\kappa(x-x_0)} e^{\frac{\kappa L_m}{2}} - e^{-\kappa(x-x_0)} e^{-\frac{\kappa L_m}{2}}] \\ -ie^{-i\chi_R} e^{-i\frac{2m_z(x_2-x)}{\hbar v_F}} u_{0\uparrow} \\ ie^{-i\chi_R} e^{-i\frac{2m_z(x_2-x)}{\hbar v_F}} u_{0\downarrow} \end{pmatrix} & x_1 < x < x_2, \\ \begin{pmatrix} \frac{e^{i\Gamma_0} e^{-i\chi_z}}{\sqrt{T_0}} e^{ik_F x} \\ ie^{-ik_F x}\sqrt{\frac{1-T_0}{T_0}} e^{i(2k_F x_0+\phi)} e^{-i\chi_z} \\ -ie^{-i\chi_R} u_{0\uparrow} \\ ie^{-i\chi_R} u_{0\downarrow} \end{pmatrix} & x > x_2, \end{cases} \tag{A1}$$

where $\kappa = \sqrt{m_\parallel^2 - \mu^2}/(\hbar v_F)$, $\tilde{\theta}_0 = \arccos(\mu/m_\parallel)$, $T_0 = (1 + \frac{\sinh^2[\kappa L_m]}{\sin^2\tilde{\theta}_0})^{-1}$, $\Gamma_0 = \arctan(\frac{1}{\tan\tilde{\theta}_0}\tanh[\kappa L_m]) - k_F L_m$, $\chi_z = m_z L_m/(\hbar v_F)$, with $L_m = x_2 - x_1$ and $x_0 = (x_1 + x_2)/2$. The second state corresponds to the reverse process of injecting a Cooper pair from the superconductor into the normal region. We call this state φ_{1^c} and it is simply given by $\varphi_{1^c} = \mathcal{C}\varphi_1$, with $\mathcal{C} = \mathcal{K}\tau_y \otimes \sigma_y$ the charge conjugation operator. From these two charge-conjugated scattering states one can construct two arbitrary independent Majorana wave functions of the form $\varphi_\pm = \alpha_\pm\varphi_1 + \alpha_\pm^*\varphi_{1^c}$. A suitable choice of $\alpha_\pm$ leads to two Majorana states localized on either side of the F domain. We found

$$\alpha_\eta = \frac{e^{-i(k_F x_1 - \chi_z - \chi_R/2)} e^{-i\eta\tilde{\theta}_0/2} e^{-\eta\kappa L_m/2}}{2\cosh(\kappa L_m/2)}, \quad \eta = \pm. \tag{A2}$$

[1] A. Y. Kitaev, Phys.-Usp. **44**, 131 (2001).
[2] E. Lieb, T. Schultz, and D. Mattis, Ann. Phys. **16**, 407 (1961).
[3] Y. Oreg, G. Refael, and F. von Oppen, Phys. Rev. Lett. **105**, 177002 (2010).
[4] R. M. Lutchyn, J. D. Sau, and S. Das Sarma, Phys. Rev. Lett. **105**, 077001 (2010).
[5] V. Mourik, K. Zuo, S. M. Frolov, S. R. Plissard, E. P. A. M. Bakkers, and L. P. Kouwenhoven, Science **336**, 1003 (2012).
[6] L. P. Rokhinson, X. Liu, and J. K. Furdyna, Nat. Phys. **8**, 795 (2012).
[7] A. Das, Y. Ronen, Y. Most, Y. Oreg, M. Heiblum, and H. Shtrikman, Nat. Phys. **8**, 887 (2012).
[8] K. T. Law, P. A. Lee, and T. K. Ng, Phys. Rev. Lett. **103**, 237001 (2009).
[9] E. J. H. Lee, X. Jiang, R. Aguado, G. Katsaros, C. M. Lieber, and S. De Franceschi, Phys. Rev. Lett. **109**, 186802 (2012).
[10] D. Bagrets and A. Altland, Phys. Rev. Lett. **109**, 227005 (2012).
[11] J. Liu, A. C. Potter, K. T. Law, and P. A. Lee, Phys. Rev. Lett. **109**, 267002 (2012).
[12] D. Rainis, L. Trifunovic, J. Klinovaja, and D. Loss, Phys. Rev. B **87**, 024515 (2013).
[13] H. O. H. Churchill, V. Fatemi, K. Grove-Rasmussen, M. T. Deng, P. Caroff, H. Q. Xu, and C. M. Marcus, Phys. Rev. B **87**, 241401 (2013).
[14] E. J. H. Lee, X. Jiang, M. Houzet, R. Aguado, C. M. Lieber, and S. De Franceschi, Nat. Nano **9**, 79 (2014).
[15] D. Chevallier, D. Sticlet, P. Simon, and C. Bena, Phys. Rev. B **85**, 235307 (2012).
[16] J. Klinovaja and D. Loss, Phys. Rev. B **86**, 085408 (2012).
[17] L. Fidkowski, J. Alicea, N. H. Lindner, R. M. Lutchyn, and M. P. A. Fisher, Phys. Rev. B **85**, 245121 (2012).
[18] I. Knez, R.-R. Du, and G. Sullivan, Phys. Rev. Lett. **109**, 186603 (2012).
[19] S. Hart, H. Ren, T. Wagner, P. Leubner, M. Mühlbauer, C. Brüne, H. Buhmann, L. W. Molenkamp, and A. Yacoby, arXiv:1312.2559.
[20] C. L. Kane and E. J. Mele, Phys. Rev. Lett. **95**, 146802 (2005).
[21] C. L. Kane and E. J. Mele, Phys. Rev. Lett. **95**, 226801 (2005).
[22] C. Wu, B. A. Bernevig, and S.-C. Zhang, Phys. Rev. Lett. **96**, 106401 (2006).
[23] M. König, S. Wiedmann, C. Brüne, A. Roth, H. Buhmann, L. W. Molenkamp, X.-L. Qi, and S.-C. Zhang, Science **318**, 766 (2007).
[24] I. Knez, R.-R. Du, and G. Sullivan, Phys. Rev. Lett. **107**, 136603 (2011).
[25] A. Kitaev, in *American Institute of Physics Conference Series*, edited by V. Lebedev and M. Feigel'Man (American Institute of Physics, Melville, NY, 2009), Vol. 1134, pp. 22–30.
[26] L. Fu and C. L. Kane, Phys. Rev. B **79**, 161408 (2009).
[27] A. M. Black-Schaffer and J. Linder, Phys. Rev. B **83**, 220511 (2011).
[28] C. W. J. Beenakker, D. I. Pikulin, T. Hyart, H. Schomerus, and J. P. Dahlhaus, Phys. Rev. Lett. **110**, 017003 (2013).
[29] M. Houzet, J. S. Meyer, D. M. Badiane, and L. I. Glazman, Phys. Rev. Lett. **111**, 046401 (2013).
[30] S. Barbarino, R. Fazio, M. Sassetti, and F. Taddei, New J. Phys. **15**, 085025 (2013).
[31] S. feng Zhang, W. Zhu, and Q. feng Sun, J. Phys.: Condens. Matter **25**, 295301 (2013).
[32] L. Jiang, D. Pekker, J. Alicea, G. Refael, Y. Oreg, A. Brataas, and F. von Oppen, Phys. Rev. B **87**, 075438 (2013).
[33] S. Mi, D. I. Pikulin, M. Wimmer, and C. W. J. Beenakker, Phys. Rev. B **87**, 241405 (2013).
[34] Everywhere in the paper $\sigma_x,\sigma_y,\sigma_z$ are Pauli matrices acting on spin degrees of freedom while τ_x,τ_y,τ_z are Pauli matrices acting on Nambu (particle-hole) degrees of freedom.
[35] P. De Gennes, *Superconductivity of Metals and Alloys*, Advanced Book Classics (Perseus Books, New York, 1999).
[36] M. J. M. de Jong and C. W. J. Beenakker, Phys. Rev. Lett. **74**, 1657 (1995).
[37] F. Taddei, F. Giazotto, and R. Fazio, J. Comput. Theor. Nanosci. **2**, 329 (2005).
[38] A. I. Buzdin, Rev. Mod. Phys. **77**, 935 (2005).
[39] T. Yokoyama, Y. Tanaka, and J. Inoue, Phys. Rev. B **72**, 220504 (2005).
[40] O. Dimitrova and M. Feigel'man, J. Exp. Theor. Phys. **102**, 652 (2006).
[41] C. Chamon, R. Jackiw, Y. Nishida, S.-Y. Pi, and L. Santos, Phys. Rev. B **81**, 224515 (2010).
[42] P. Adroguer, C. Grenier, D. Carpentier, J. Cayssol, P. Degiovanni, and E. Orignac, Phys. Rev. B **82**, 081303 (2010).
[43] D. M. Badiane, L. I. Glazman, M. Houzet, and J. S. Meyer, C. R. Phys. **14**, 840 (2013).
[44] C. W. J. Beenakker, in *Mesoscopic Quantum Physics*, edited by E. Akkermans, G. Montambaux, J.-L. Pichard, and J. Zinn-Justin (North-Holland, Amsterdam, 1994).
[45] G. Dolcetto, N. Traverso Ziani, M. Biggio, F. Cavaliere, and M. Sassetti, Phys. Rev. B **87**, 235423 (2013).
[46] D. L. Maslov, M. Stone, P. M. Goldbart, and D. Loss, Phys. Rev. B **53**, 1548 (1996).
[47] F. Crépin and B. Trauzettel, Phys. Rev. Lett. **112**, 077002 (2014).
[48] I. Kulik, Sov. Phys. JETP **30**, 944 (1970).
[49] C. W. J. Beenakker, Phys. Rev. Lett. **67**, 3836 (1991).
[50] H.-J. Kwon, K. Sengupta, and V. M. Yakovenko, Eur. Phys. J. B **37**, 349 (2004).